Journal of Materials Chemistry C

View article online
10.1039/C7TC05562E

Dielectric elastomer actuators with increased dielectric permittivity and low leakage current capable of suppressing electromechanical instability

Philip Caspari,[a,b] Simon J. Dünki,[a,b] Frank A. Nüesch,[a,b] Dorina M. Opris[a]*

[a.] *Swiss Federal Laboratories for Materials Science and Technology Empa, Laboratory for Functional Polymers, Überlandstr. 129, CH-8600, Dübendorf, Switzerland, E-mail: dorina.opris@empa.ch*

[b.] *École Polytechnique Fédérale de Lausanne (EPFL), Institut des matériaux, Station 12, CH 1015, Lausanne, Switzerland*

Electronic Supplementary Information (ESI) available: 1H NMR, 13C NMR, TGA, DSC, GPC, IS, Tensile tests, actuators, two videos with actuators. See DOI: 10.1039/x0xx00000x

Dielectric elastomers with increased dielectric permittivity (ε'), excellent insulating and mechanical properties have a broad application potential ranging from flexible electronics to dielectric elastomer transducers. Up to date, several reports exist on elastomers with increased permittivity, but unfortunately in most cases this increase in permittivity is associated with an increase in conductivity, which detrimentally affects the insulating properties, such as leakage current and dielectric breakdown. Here, novel polysiloxane based elastomers were prepared in three steps starting from a silanol end-terminated poly(methylvinyl)siloxane, whose vinyl groups were reacted with alkyl thiols *via* thiol-ene reaction. The resulting polymers were cross-linked using condensation reactions and the dielectric, mechanical and electromechanical properties were evaluated. Eventually, an optimized material with a relative permittivity of ε' = 5.4, a conductivity of 4×10^{-11} S cm^{-1}, a storage modulus of 300 kPa, and a mechanical loss factor below 0.05 was achieved. Actuators constructed from this optimized material showed no electromechanical instability in the absence of prestrain. An area actuation strain of about 200% at an electric field of 53 V μm^{-1} was achieved. This excellent electromechanical behavior can be rationalized by the increased permittivity due to the thioether side chain and its favorable strain-stiffening effect on the material when crosslinked with polar alkoxysilanes. The actuators gave a stable

lateral actuation strain of 10% for more than 50000 cycles when subjected to an electric field of 27 V μm^{-1} at a modulation frequency of 8 Hz. Due to the combined properties of this material such as a low leakage current density of 0.5 $\mu A\ cm^{-2}$ at 27 V μm^{-1}, an attractively low glass transition temperature, a very fast electromechanical response and an increased permittivity, the dielectric elastomers developed in this work may be considered as future replacement for polydimethylsiloxane elastomers in dielectric elastomer transducers.

Introduction

Dielectric elastomers (DEs) with increased dielectric permittivity and high dielectric breakdown field are important materials for future electromechanical transducers (DETs).[1-7] Such devices can convert electrical into mechanical energy (actuator mode)[1-5] or *vice versa* (generator mode)[6] and can sense changes in pressure due to capacitance changes with strain.[7] While for the last application, the dielectric breakdown is not a critical parameter, for the first two applications, elastomers with high breakdown field are advantageous.[8] Unfortunately, dielectric elastomer actuators (DEAs) are prone to electromechanical instability (EMI), which sets in at an area actuation strain of about 40%.[9-12] As the voltage U increases and the thickness of the dielectric elastomer d decreases, the electric field U/d increases rapidly, which leads to a positive feedback of the dielectric elastomer, also known as *pull-in* or *snap-through* instability. This effect may cause electrical breakdown of the dielectric elastomer.[10] According to Stark and Garton, dielectric breakdown is proportional to the square root of the elastic modulus.[8] It has been shown that the stress-strain characteristics of an elastomer can be tuned such as to suppress EMI in actuators.[13, 14] This can be achieved with materials that show a strain-stiffening effect, *e.g.* a sharp increase in the elastic modulus above a certain strain.[11] This concept was nicely confirmed experimentally using prestrained VHB foil for which giant area expansions as high as 1600% were reported.[15-17] While prestraining the films can increase the actuation strain, the energy density and allows for actuation in a predetermined direction, several disadvantages can be noted.[1] Firstly, prestraining the elastomer implies an additional processing step and is therefore time consuming. Secondly, it requires rigid frames to maintain the tension in the films, which increases the volume and the mass of the device.[18,19] Thirdly, actuator life time is significantly reduced due to creep and fatigue of the elastomer. Therefore, it would be advantageous to have elastomers capable of suppressing EMI

while unprestrained. Unfortunately, most available elastomers such as polydimethylsiloxanes and acrylates show strain-stiffening only at very high strains and thus actuation is hampered by EMI.

It was proposed that interpenetrated polymer networks, swelled networks, or cross-linked bottle-brush polymers may be able to overcome the EMI.[11] Meanwhile, novel DE materials and composites have been developed showing high actuation in the absence of prestrain. For example, block copolymers swollen with an aliphatic oil, an interpenetrated network based on prestrained VHB and a poly(1,6-hexanediol diacrylate) network formed inside[20] as well as interpenetrating networks composed of long and short polymer chains were shown to be capable of overcoming EMI.[20-23] Most recently, cross-linked bottlebrush polymers were introduced as DE materials for actuators.[24] Bottlebrush elastomers are inherently prestrained due to the steric demand of the side chains. By varying side chain length, grafting density, and cross-link density, elastomers with elastic moduli that vary from 1 MPa to 100 Pa with a relative permittivity of $\varepsilon' = 2.95$ were prepared.

Despite the substantial amount of research on high permittivity elastomers, none of the reported materials combines a high permittivity with low glass transition temperature (T_g) and favorable mechanical properties that suppress EMI.[25-28] To increase the permittivity, composites containing polarizable fillers such as conductive particles and high permittivity ceramics as well as low T_g polar polymers have been used.[28] The increase in permittivity ε' is usually accompanied by an increase in conductivity.[29, 30] Actuators constructed with such materials have usually a low breakdown field and thus suffer premature breakdown. Madsen *et al.* reported that silicones modified with chloropropyl groups have $\varepsilon' = 4.7$ and an increased dielectric breakdown field, which according to the authors is due to the presence of chlorine in the materials.[31] By replacing the chloropropyl groups with chloromethyl groups, elastomers with even higher dielectric permittivity of $\varepsilon' = 6$ and a breakdown strength of 60 V μm^{-1} were achieved.[32] While none of these materials was evaluated in electromechanical tests, it seems that the presence of chlorine increases the dielectric strength of silicone elastomers.

We have recently introduced a novel elastomer for actuators, a polysiloxane modified with butylthioether side groups. Its dielectric permittivity is $\varepsilon' = 4.3$, higher as compared to regular polydimethylsiloxane (PDMS) elastomers ($\varepsilon' \sim 3$) and it actuates at lower electric field. However, the dielectric breakdown occurred at 23 V μm^{-1}.[29, 33, 34]

Encouraged by the theoretical predictions and the outstanding performance of bottle brush polyacrylate actuators,[24] we developed a high permittivity silicone elastomer which is capable of suppressing EMI while unprestrained. It also has a fast response time which is comparable to PDMS

elastomers.[35] To achieve this material, we first investigated the influence of alkyl-thioether side groups of different lengths grafted on the polysiloxane on T_g, mechanical, dielectric, and electromechanical properties. Our approach consisted of optimizing the length of the alkyl chain allowing the formation of materials with good mechanical properties and maximum increase in permittivity while suppressing electromechanical instability. This allowed us to develop a silicone elastomer that showed unprecedentedly high actuation strain, fast electromechanical response and high reliability. Because of its low leakage current and low glass transition temperature, this material can be considered as a serious alternative to regular PDMS elastomers for DE applications.

Experimental Section

Materials and Characterization

Materials and Methods

Unless otherwise stated, all chemicals were reagent grade and used without purification. 1,3,5,7-Tetramethyl-1,3,5,7-tetravinyl cyclotetrasiloxane (**V4**), (25-35% methylhydrosiloxane)-dimethylsiloxane (AB109380) **A** and polydimethylsiloxane (AB116665, $M_n = 90.000$ g mol^{-1}, $M_w = 130.000$ g mol^{-1}) were purchased from ABCR. 2,2-Dimethoxy-2-phenylacetophenone (DMPA), ethanethiol, 1-propanethiol, 1-butanethiol, 1-hexanethiol, 1-octanethiol, tetramethylammonium hydroxide 25% in MeOH (TMAH), 3-chlorpropyltriethoxysilane, 2-cyaonoethyltriethoxysilane, and dibutyltin dilaurate were purchased from Aldrich. Methanol and tetrahydrofuran were purchased from VWR. The synthesis of polymethylvinylsiloxane **P0** was done according to the literature ($M_n = 91.000$ g mol^{-1}, $M_w = 176.000$ g mol^{-1}, PDI = 1.93). Films of Elastosil®Film (200 µm, 100 µm, 50 µm, 20 µm) were provided by DRAWIN Vertriebs-GmbH, Riemerling. PVA was purchased from Swiss Composite. Photoreactions were conducted with a UVAHAND 250 GS H1 mercury vapor UV lamp from Dr. Hoenle AG.

^{1}H and ^{13}C NMR spectra were recorded at 298 K on a Bruker Avance 400NMR spectrometer using a 5 mm broadband inverse probe at 400.13 and 100.61 MHz, respectively. Chemical shifts (δ) in ppm were calibrated to residual solvent peaks ($CDCl_3$: δ = 7.26 and 77.16 ppm).

Gel permeation chromatograms were recorded using an Agilent 1100 Series HPLC (Columns: serial coupled PSS SDV 5 m, 100A and PSS SDV 5 m, 1000A, detector: DAD, 235 nm and 360 nm; refractive index), with THF as mobile phase. PDMS standards were used for calibration and toluene as an internal standard.

Differential scanning calorimetry (DSC) investigations were undertaken on a Pyris Diamond DSC (Perkin Elmer USA) instrument under a nitrogen flow (50 ml × min^{-1}), in aluminum crucibles shut with pierced lids and using a 10 mg sample mass.

The tensile tests were performed on a Zwick Z010 tensile test machine with a crosshead speed of 50 mm min^{-1} (278% min^{-1}). Tensile test specimens with a gauge width of 2 mm and a gauge length of 18 mm were prepared by die cutting. The strain was determined using a longitudinal strain extensometer. The curves were averaged from 3 different samples. The elastic modulus *Y* was determined from the slope of the stress–strain curves using a linear fit to the data points within ±5% strain. Dynamic mechanical analysis was carried out on a RSA 3 DMA from TA Instruments. Stripes of 10 mm × 20 mm were measured under a dynamic load of 2 g, at 2% strain in the frequency range of 0.05–10 Hz at 25 °C. $Tan(\delta)_{DMA}$ is given as the fraction of imaginary and real elastic modulus at 2% strain.

Permittivity measurements were performed in the frequency range from 10^{-1} Hz to 10^{6} Hz using a Novocontrol Alpha-A frequency analyzer. The VRMS (root mean square voltage) of the probing AC electric signal applied to the samples was 1 V. Au electrodes with a thickness of 20 nm were sputtered on both sides of the film. The permittivity ε' was determined from the capacitance $C= \varepsilon'\varepsilon_0 A/d$, where *A* is the electrode area, *d* is the thickness of the film, and ε_0 is the vacuum permittivity. The thickness of the film was measured by a micrometer gauge with an uncertainty of ±5 µm. For temperature variable dielectric spectroscopy (BDS) measurements a high impedance Alpha Analyzer combined with a Quatro temperature controller (both from Novocontrol) has been employed to cover a broad frequency and temperature range from 10^{-1} Hz to 10^{6} Hz and from -150 to 60 °C, respectively. Two stainless steel discs with a diameter of 20 mm served as electrodes which were separated by three glass fibers with a diameter of 100 µm± 5 µm. The samples were annealed at 80 °C for 18 h at 10 mbar to remove any residual solvents before isothermal measurements were performed. During measurement the samples were kept in dry nitrogen atmosphere.

Electromechanical tests were performed using circular membrane actuators, for which the films were fixed between two circular frames. Circular electrodes (8 mm diameter) of carbon black powder were applied to each side of the film. A custom-made radial stretching device was used to prestrain the samples. Samples **E2**, **E3**, **Er**, **En-X-Y**, were prestrain biaxially by 7.5%, while sample **E3-Cl-20** different biaxial prestrains were used: 0%, 22.5, and 30%. A FUG HCL- 35-12500 high voltage source served as power supply for actuator tests. The voltage was increased by 50 V steps every 2 s up to maximum 5.6 kV. The actuation strain was measured optically as the extension of the diameter of the electrode area *via* a digital camera, using an edge detection tool of a LabView program to detect the boundary

between the black electrode area and the transparent silicone film. The maximum resolution of LabView was 30 measurements per second. Current leakage was measured up to a voltage of 5 kV.

Synthesis of Pn

To a solution of **P0** (20.01 g, 232.2 mmol of vinyl groups, 1 eq) in dry THF (200 ml), alkylthiol (464.5 mmol, 2.0 eq thiol, 28.80 g of ethanethiol for **P2**, 35.30 g of 1-propanethiol for **P3**, 41.81 g of 1-butanethiol for **P4**, 54.81 g of 1-hexanethiol for **P6**, 67.82 g 1-octanethiol for **P8**, 80.98 g 1-decanethiol for **P10,** 93.83 g 1-dodecanethiol for **P12,** respectively) and DMPA (560 mg, 2.18 mmol, 0.009 eq) were added. The solution was degassed by three freeze-pump-thaw cycles and irradiated with UV light for 5 min. It was then concentrated *in vacuo* to about 50 ml. To this concentrated solution, methanol was added whereupon the polymer precipitated. The polymer was redissolved in THF and again precipitated with methanol. The dissolution/precipitation process was repeated three times. The highly viscous liquids were then dried at 10^{-2} mbar at 60 °C to obtain **P2**-**P8** in 90-95% yield.

P2: ^{1}H NMR (400 MHz, $CDCl_3$, δ): 2.58 – 2.50 (m, 4H, -CH_2-S-CH_2-), 1.24 (t, ^{3}J= 7.4 Hz, 3H, -CH_2-CH_3), 0.92 – 0.86 (m, 2H, Si-CH_2-CH_2-), 0.13 (s, 3H, Si-CH_3); ^{13}C NMR (100 MHz, $CDCl_3$, δ): 25.9, 25.8, 18.4, 14.8, 0.0.

P3: ^{1}H NMR (400 MHz, $CDCl_3$, δ): 2.57 – 2.48 (m, 4H, -CH_2-S-CH_2-), 1.60 (tq, ^{3}J= 7.3 Hz, ^{3}J= 7.3 Hz, 2H, -CH_2-CH_3), 0.99 (t, ^{3}J= 7.3 Hz, 3H, -CH_2-CH_3), 0.92 – 0.87 (m, 2H, Si-CH_2-CH_2-), 0.14 (s, 3H, Si-CH_3); ^{13}C NMR (100 MHz, $CDCl_3$, δ): 34.2, 26.5, 23.0, 18.6, 13.8, 0.1.

P4: ^{1}H NMR (400 MHz, $CDCl_3$, δ): 2.60 – 2.48 (m, 4H, -CH_2-S-CH_2-), 1.60 – 1.52 (m, 2H, CH_2-CH_2-CH_3), 1.46 – 1.37 (m, 2H, CH_2-CH_3), 0.94 – 0.87 (m, 5H, Si-CH_2-, CH_2-CH_3), 0.14 (s, 3H, Si-CH_3); ^{13}C NMR (100 MHz, $CDCl_3$, δ): 31.9, 31.8, 22.2, 18.5, 13.9, 0.1.

P6: ^{1}H NMR (400 MHz, $CDCl_3$, δ): 2.57-2.49 (m, 4H, -CH_2-S-CH_2-), 1.60-1.53 (m, 2H, CH_2-CH_2-CH_3), 1.42 – 1.35 (m, 2H, CH_2-CH_3), 1.33 – 1.25 (m, 4H, -CH_2-CH_2-CH_2-CH_2-CH_3), 0.90 – 0.87 (m, 5H, Si-CH_2-, CH_2-CH_3), 0.14 (s, 3H, Si–CH_3); ^{13}C NMR (100 MHz, $CDCl_3$, δ): 32.3, 31.7, 29.8, 28.9, 26.6, 22.8, 18.5, 14.3, 0.2.

P8: ^{1}H NMR (400 MHz, $CDCl_3$, δ): 2.57-2.49 (m, 4H, -CH_2-S-CH_2-), 1.60-1.53 (m, 2H, CH_2-CH_2-CH_3), 1.42 – 1.33 (m, 2H, CH_2-CH_3), 1.27 (br s, 8H, -S-CH_2-(CH_2)$_4$-CH_2-CH_2-CH_3), 0.92 – 0.85 (m, 5H, Si-CH_2-, CH_2-CH_3),

0.13 (s, 3H, Si–CH_3); ^{13}C NMR (100 MHz, $CDCl_3$, δ): 32.3, 32.0, 29.8, 29.5, 29.4, 29.3, 26.6, 22.9, 18.5, 14.3, 0.1.

P10: ^{1}H NMR (400 MHz, $CDCl_3$, δ): 2.58-2.48 (m, 4H, -CH_2-S-CH_2-), 1.60-1.52(m, 2H, CH_2-CH_2-CH_3), 1.44 – 1.33 (m, 2H, CH_2-CH_3), 1.29 (br s, 12H, -S-CH_2-(CH_2)$_6$-CH_2-CH_2-CH_3), 0.92 – 0.85 (m, 5H, Si-CH_2-, CH_2-CH_3), 0.13 (s, 3H, Si–CH_3); ^{13}C NMR (100 MHz, $CDCl_3$,δ): 32.31, 32.07, 29.80, 29.55, 29.51, 29.27, 26.60, 22.80, 18.49, 14.24, 0.08.

P12: ^{1}H NMR (400 MHz, $CDCl_3$, δ): 2.56-2.48 (m, 4H, -CH_2-S-CH_2-), 1.60-1.53 (m, 2H, CH_2-CH_2-CH_3), 1.43 – 1.34 (m, 2H, CH_2-CH_3), 1.25 (br s, 16H, -S-CH_2-(CH_2)$_4$-CH_2-CH_2-CH_3), 0.92 – 0.85 (m, 5H, Si-CH_2-, CH_2-CH_3), 0.13 (s, 3H, Si–CH_3); ^{13}C NMR (100 MHz, $CDCl_3$, δ): 32.33, 32.08, 29.90, 29.88, 29.85, 29.81, 29.56, 29.55, 29.32, 26.62, 22.86, 18.52, 14.28, 0.09.

General synthesis of the elastomers

A solution of **Pn** (4 g), cross-linker **A**, **Cl-CL**, or **CN-CL** (for the amount used, see Table 1), and dibutyltin dilaurate (80 µl, 0.056 g, 0.1 mmol) in THF (4 ml) was casted on a PTFE or PVA/glass substrate by doctor blade technique. The films were stored in a closed chamber at ambient temperature of 25 °C and humidity 30% for 48 h. The films were dried at 70 °C *in vacuo* for 12 h before further testing.

Table 1. The amount of reagents used for the synthesis of **En** and **En-X-Y**.

Entry	Polymer	Polymer [g]	**A** [ml]	**Cl-CL** [g]	**CN-CL** [g]
Er	PDMS	4	0.21	-	-
E2	**P2**	4	0.13	-	-
E3	**P3**	4	0.13	-	-
E4	**P4**	4	0.12	-	-
E6	**P6**	4	0.11	-	-
E8	**P8**	4	0.09	-	-
E10	**P10**	4	0.08	-	-
E12	**P12**	4	0.07	-	-
Er-Cl-33	PDMS	4	-	2 g	-
Er-Cl-20	PDMS	4	-	1 g	-
E2-Cl-33	**P2**	4	-	2 g	-
E2-Cl-20	**P2**	4	-	1 g	-
E3-Cl-33	**P2**	4	-	2 g	-
E3-CL-20	**P3**	4	-	1 g	-
E2-CN-33	**P2**	4	-	-	2 g
E2-CN-20	**P2**	4	-	-	1 g
E3-CN-	**P3**	4	-	-	2 g

33 E3-CN-20	**P3**	4	-	-	1 g

Results and discussion

A series of polysiloxanes, **P_n**, modified with alkyl-thioethers of different length, where 'n' refers to the number of C-atoms in the alkyl chains, was synthesized starting from a silanol-terminated poly(methylvinyl)siloxane **P_0** (M_n = 91.000 g mol^{-1}) *via* photoinduced thiol-ene addition with various alkyl thiols (Scheme 1, Figure S1 and S2). All reactions were carried out with the same batch of P_0. The disappearance of the vinyl groups in the ^{1}H NMR spectra of the final products was used as a clear indication for the success of the post-polymerization modification (Figure S3-S16). Differential scanning calorimetry (DSC) was conducted to investigate the influence of the alkyl-thioether length on both T_g and melting temperature (T_m) (Figures S17-S22). The results are compiled in Table 2. While polymers **P2**, **P3**, **P4**, and **P6** show a glass transition, they do not exhibit a melt transition. In contrast, polymers **P8**, **P10**, and **P12** do not undergo a glass transition, however, they do melt.

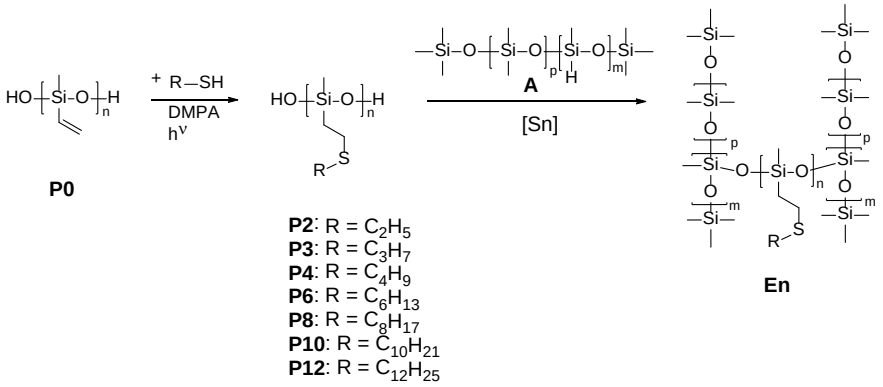

Scheme 1 Synthesis of polysiloxanes **Pn** modified with alkyl thioether groups and their cross-linking with (methylhydrosiloxane)-dimethylsiloxane-copolymer A (m: 25-30%; p: 75-70%) *via* tin-catalyzed dehydrogenative coupling reaction.

All polymers of Table 2 were cross-linked using (methylhydrosiloxane)-dimethylsiloxane-copolymer **A** cross-linker (m: 25-30%; p: 75-70%) to give materials **En**, whereby 'E' indicates that these products are elastomers and 'n' refers to the number of C-atoms in the lateral substituents. This was achieved with a tin-catalyzed dehydrogenative coupling reaction between the silanol end groups of the polymers and the hydrosilyl groups of **A** (Scheme 1). As reference material, **Er** was used which was obtained by cross-linking a silanol end-terminated polydimethylsiloxane (PDMS, M_n = 90.000 g mol^{-1}) with **A** under exact

same conditions. The amount of cross-linker **A** was in all cases very low (5-2 wt-%) so that its influence on permittivity could be neglected. It was noted that the condensation reaction was slowed down for the polymers that carry a shorter thioalkyl group and thus a higher content of sulfur.

First, it was checked whether the elastomers **En** form free standing films. As this was the case only for the networks **E2**-**E8**, only those materials were further investigated. The dielectric properties of **En** and **Er** were analyzed by impedance spectroscopy. As expected, an increase in the dielectric permittivity with increasing sulfur content in materials **En** was observed (Figure 1). Materials **E2** and **E3** had ε' = 5.4 and 5.2, respectively, whereas **Er** had ε'= 2.8. When the alkyl chain length in polymers **En** was further increased, the permittivity decreased. An increase in conductivity with increasing the sulfur content was observed from 2×10^{-14} S cm^{-1} for **Er** to 9.8×10^{-12} S cm^{-1} for **E3** and 3.56×10^{-11} S cm^{-1} for **E2**. The dielectric losses at high frequencies were also low, but increased with decreasing frequency due to electrode polarization.

Table 2 Transition temperatures observed for **Pn**, the ΔC_p of the transitions, M_w, M_n, and PDI.

Pn	T [°C]			ΔC_p [J g^{-1} °C^{-1}]		M_w [g mol^{-1}]	M_n [g mol^{-1}]	PDI
	Tg[a)]	T_m[a)]	cooling[b)]	2nd heating	cooling[b)]			
P2	-93.3	-	-102.1	0.365	0.503	340.000	75.000	4.5
P3	-96.9	-	-103.1	0.387	0.499	225.000	90.000	2.5
P4	-97.5	-	-	0.395	-	220.000	100.000	2.2
P6	-92.9	-	-99.6	0.452	0.658	100.000	40.000	2.5
P8	-	-48.5	-63.1 (T_c)	-	-	640.000	55.000	11.6
P10	-	-9.3	-23.1 (T_c)	-	-	150.000	40.000	3.8
P12	-	16.2	1.4 (T_c)	-	-	350.000	60.000	5.8

a) Data from second heating cycle. b) Data from first cooling. ΔC_p is heat capacity.

View article online
10.1039/C7TC05562E

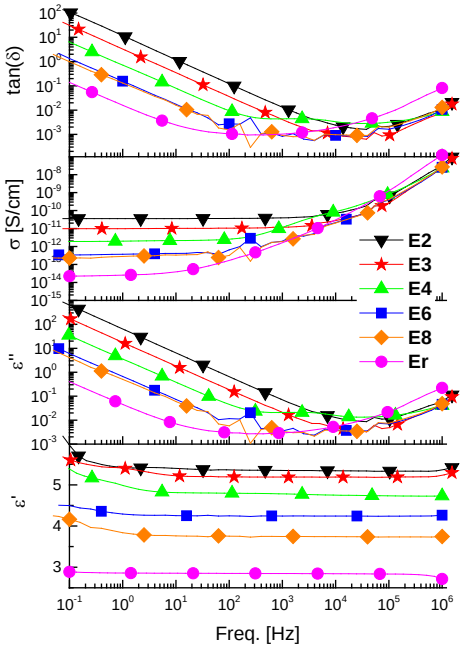

Fig. 1 Dielectric properties of **E2**-**E8** and **Er**.

The mechanical properties of **En** were evaluated in tensile tests. The strain at break for all materials was below 200% and decreased with increasing alkyl chain length (Figure 2, Table 3). The elastic moduli of **En** slightly decreased at small strains and remained unchanged above a certain strain level, whereas the elastic moduli of the reference **Er** decreased for strains between 0% and 65%, remained almost unchanged up to 120%, and increased at strains above 120% (Figure 2 middle). **En** were further evaluated as dielectric in actuators for which 7.5% biaxial prestrain was used. Attempts to construct actuators from materials **E4**-**E8** were not successful as these materials were rather fragile and ruptured during manipulation. The mechanical properties of materials **E2** and **E3** allowed to construct circular actuator devices. Material **E2** gave 12% lateral strain at 15 V μm^{-1}, whereas **E3** gave 9.5% strain at 19 V μm^{-1} (Figure 2 right). Despite the low dielectric breakdown of the actuators constructed from **E2** and **E3**, their maximum actuation was higher as compared to **Er** which gave only 7% lateral actuation at much higher electric field of 66 V μm^{-1}. These results show the positive effect of the thioether side group on the electromechanical sensitivity ε/Y which enables high actuation strains of **E2** and **E3** at relatively low electric fields. However, the actuators' dielectric breakdown of 15 V μm^{-1} and 19 V μm^{-1} for **E2** and **E3**, respectively, is too low.

View article online
10.1039/C7TC05562E

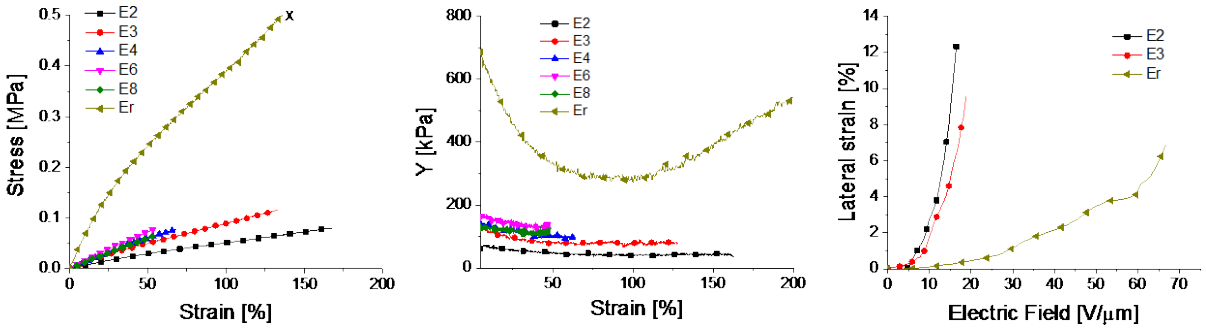

Fig. 2 Stress-strain curves (left) and elastic moduli at different strains (middle) of **En** at a stretch rate of 50 mm min^{-1} as well as lateral actuation strain of **E2**, **E3** and **Er** as function of applied electric field (right). The stress-strain curves were averaged from 3 different samples.

Table 3 Dielectric, mechanical, and electromechanical properties of **E2**-**E8** and **Er**.

Entry	ε'@ 10^6 Hz	σ@ 10^{-1} Hz	tan(δ)@ 10^6 Hz	$Y_{10\%}$ [kPa]	s_{max} [%]	$s_{act,max}$ [%]	$E_{b,act}$ [V µm^{-1}]
Er	2.8	$2\ 10^{-14}$	0.08	600	300	7%	66
E2	5.4	$3.56\ 10^{-11}$	0.013	70	190	12%	15
E3	5.2	$9.8\ 10^{-12}$	0.010	120	150	10%	19
E4	4.7	$1.9\ 10^{-12}$	0.008	135	71	-	-
E6	4.2	$3\ 10^{-13}$	0.010	160	58	-	-
E8	3.7	$2\ 10^{-13}$	0.013	130	54	-	-

To evaluate whether **P2** and **P3** can be cross-linked to elastomers with improved properties, other cross-linking reactions were explored. It is known that the mechanical properties of polysiloxanes can be enhanced by fillers which are either *ex situ* or are generated *in situ*.[36-38] Homogenous materials with uniformly dispersed silica particles generated in-situ *via* hydrolysis and condensation of tetraethoxysilane were reported. More recently trialkoxy(alkyl)silanes with different polar groups were used to cross-link PDMS.[33, 39] Trialkoxy(alkyl)silanes undergo condensation reactions with the silanol end-groups of the polysiloxane and also self-condensation reactions with formation of silsesquioxane structures. From all trialkoxy(alkyl)silanes used, 3-chloropropyl(triethoxy)silane (**Cl-CL**) and 2-cyanoethyl(triethoxy)silane (**CN-CL**) were found to allow formation of materials with improved dielectric and mechanical properties.[33, 40] These cross-linkers have also attractive dielectric permittivity, *e.g.* $\varepsilon' = 5.8$ for **Cl-CL** and $\varepsilon' = 12.3$ for **CN-CL** (Figure S23). Therefore, we used these two cross-linkers in two

different concentrations, 33 wt-% and 20 wt-%, respectively to cross-link **P2** and **P3**. This allowed formation of materials **En-X-Y**, where 'E' indicates that these products are elastomers, 'n' refers to the number of C-atoms of the thiol used for the functionalization of **Pn**, X refers to the type and Y refers to the wt-% of cross-linker used, respectively. For example, the cross-linking of **P2** with 33 wt-% **Cl-CL** allowed formation of material **E2-Cl-33** and with 20 wt-% **Cl-CL** the formation of material **E2-Cl-20**. Materials with attractive mechanical properties formed after cross-linking for about 48 h at ambient temperature (Table 4).

Thermal stability of **En-X-Y** was investigated by TGA (Figure S24-S35) which showed that all elastomers are stable up to 370 °C where a small amount of volatiles is removed. Above 450 °C the elastomers lose more than half of their weight. DSC investigations show that these materials have no transition at temperatures above -80 °C which is an attractive feature (Figure S36-S43).

As expected, because **E2-X-Y** has a higher content of sulfur as compared to **E3-X-Y**, its dielectric permittivity is slightly higher as compared to **E3-X-Y** (Table 4). Furthermore, the permittivity increases with increasing the content of cross-linker. The dielectric permittivity of materials **En-CN-Y** was higher as compared to materials **En-Cl-Y**, but they also showed higher conductivity at low frequencies. Table 4 summarizes several dielectric characteristics of the new materials. The highest relative permittivity of $\varepsilon' = 7.0$ (10^6 Hz) was measured for **E2-CN-33**. This material has the highest content of both sulfur and polar nitrile groups (Figure 3). Unfortunately, also the conductivity was the highest $\sigma = 10^{-11}$ S cm^{-1} at 10^{-1} Hz. When **Cl-CL** was used, the highest achieved relative permittivity was $\varepsilon' = 6.4$ for material **E2-Cl-33** which has the highest content of sulfur and chlorine. A sharp increase in permittivity at low frequencies for all materials was observed. This increase is due to electrode polarization, due to ions accumulated at the electrodes.[41] This effect is stronger for elastomers containing the nitrile functionality.

View article online
10.1039/C7TC05562E

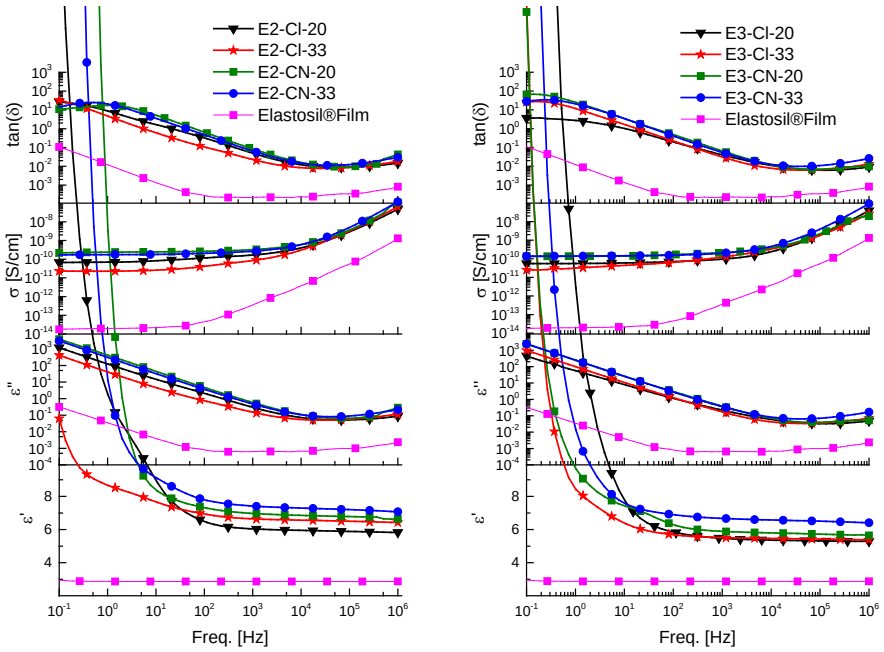

Fig. 3 Dielectric properties of materials **E2-X-Y** (left) and **E3-X-Y** (right) as well as the one of the reference Elastosil®Film.

Dynamic mechanical analysis (DMA) was used to further characterize the elastic behaviour of our materials (Figure 4). The reference material **Elastosil®Film** had the highest storage modulus and has a low loss factor *tan(δ)* which did not change in the investigated frequency range. Materials **E2-X-Y** were softer as compared to **E3-X-Y** and showed larger loss factors which increased with frequency. Particularly, **E2-CN-Y** elastomers had a *tan(δ)* higher than 0.15 at frequencies above 2 Hz, which may be an indication of poor cross-linking. Swelling extraction tests conducted on **En-X-Y** are in agreement with the DMA results (Table 4). The highest amount of extractable was found for **E2-CN-Y**. Materials **E3-X-Y** showed very good mechanical properties with *tan(δ)* below 0.1 at all frequencies, with **E3-Cl-Y** showing the best performance. Material **E3-Cl-33** had a storage modulus of about 700 kPa while **E3-Cl-20** had a storage modulus of 300 kPa. Both materials showed a mechanical loss factor below 0.05 which only slightly increased with frequency (Figure 4).

View article online
10.1039/C7TC05562E

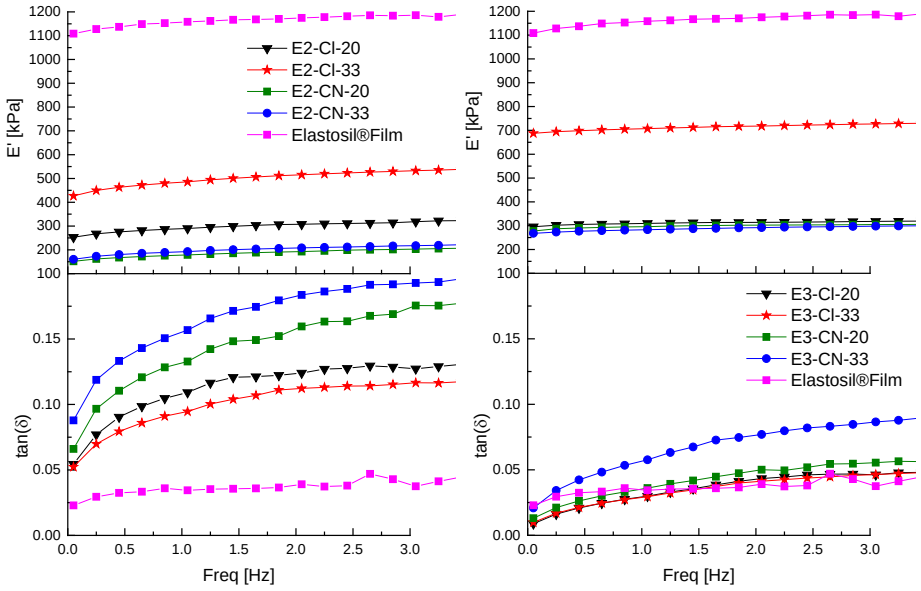

Fig. 4 Dynamic mechanical analysis of **En-X-Y** and **Er** ranging from 0.05 Hz to 3 Hz at a strain of 2%.

Table 4 Dielectric and mechanical properties of **En-X-Y** and **Er**.

Entry	ε' @ 10^6 Hz	σ @ 10^{-1} Hz	$tan(\delta)$@ 10^6 Hz	$Y_{(10\%)}$ [a] [kPa]	$Y_{50\%}$ [a] [kPa]	$Y_{100\%}$ [a] [kPa]	s_{max} [%]	$tan(\delta)$ [b] [2 Hz]	Extractable [%]
E2-Cl-20	5.8	$3\ 10^{-11}$	$5\ 10^{-2}$	330	640	1380	125	$1.2\ 10^{-1}$	17.2
E2-Cl-33	6.4	$1\ 10^{-11}$	$2\ 10^{-2}$	700	2600	-	65	$1.1\ 10^{-1}$	14.5
E2-CN-20	6.7	$1\ 10^{-10}$	$2\ 10^{-2}$	200	150	220	175	$1.6\ 10^{-1}$	27.6
E2-CN-33	7.0	$4\ 10^{-9}$	$4\ 10^{-2}$	250	220	470	190	$1.8\ 10^{-1}$	32.6
E3-Cl-20	5.4	$4\ 10^{-11}$	$2\ 10^{-2}$	370	500	1230	100	$4\ 10^{-2}$	13.4
E3-Cl-33	5.5	$4\ 10^{-11}$	$2\ 10^{-2}$	580	1380	-	60	$4\ 10^{-2}$	11.8
E3-CN-20	5.8	$1\ 10^{-10}$	$7\ 10^{-2}$	370	330	830	100	$5\ 10^{-2}$	17.8
E3-CN-33	6.3	$2\ 10^{-9}$	$3\ 10^{-2}$	250	370	-	80	$8\ 10^{-2}$	22.7
Er-Cl-20	2.9	$10\ 10^{-12}$	$2\ 10^{-3}$	500	260	190	350	$2\ 10^{-2}$	8.9
Er-Cl-33	3.4	$7\ 10^{-12}$	$2\ 10^{-3}$	530	260	170	390	$2\ 10^{-2}$	9.7
Er	2.8	$2\ 10^{-14}$	$8\ 10^{-2}$	600	320	280	300	$1\ 10^{-2}$	8.6
Elastosil® Film	2.9	$2\ 10^{-14}$	$1\ 10^{-3}$	1200	730	1040	486	$3\ 10^{-2}$	1.6

[a] The elastic moduli were determined from the slope of the stress–strain curves using a linear fit to the data points within ±5% strain. These data were averaged from 3 different samples. [b] Taken from DMA.

Figure 5 shows the unilateral stress-strain curves of **En-X-Y**. The strain at break of all materials was rather low, *e. g.* only two samples **E2-CN-20** and **E2-CN-33** showed a strain at break above 150% (Figures

S44-S60). While this property is important for DETs operated in the generator mode, in actuator devices, the strain at break is not a limiting factor. Irrespective of the type of cross-linker used, the materials got stiffer with increasing the cross-linker content with the strongest effect observed for materials **En-Cl**-Y. The elastic moduli of materials **E2-CN-Y** were almost constant with strain. Materials **E2-Cl-Y** and **E3-X-Y** showed a strong increase in the elastic moduli at strains above 50%. For example **E3-Cl-33** showed a doubling in elastic modulus from *Y*= 580 kPa at 10% strain to *Y*= 1380 kPa at 50% strain. Two reference materials **Er-Cl-20** and **Er-Cl-33** were also prepared by cross-linking a silanol terminated PDMS with 20 wt-% and 33 wt-% **Cl-CL**, respectively. During cross-linking in thin films silsesquioxane structures are *in situ* generated. While, the reference materials **Er-X-Y** were becoming softer with the strain,[33] materials **E3-X-Y** and **E2-Cl-Y** showed a synergetic effect between the thioether side groups and the *in situ* generated silsesquioxane reflected by a rapid stiffening of the materials above a certain strain (Figure 5d,e).

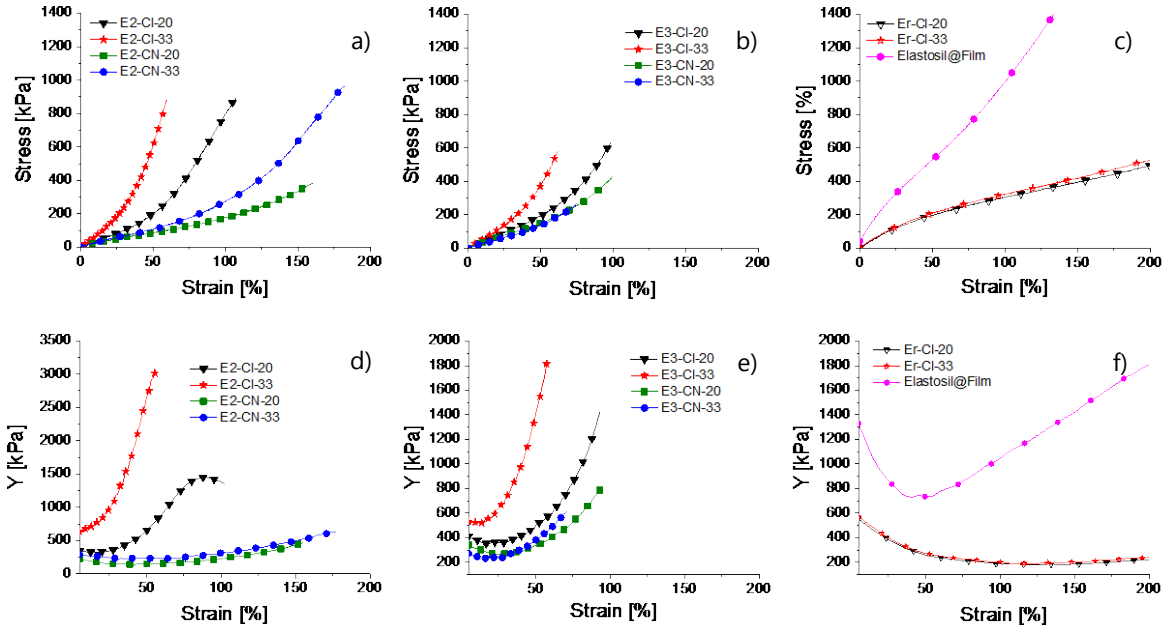

Fig. 5 Stress-strain curves for materials **E2-X-Y** (a), **E3-X-Y** (b) and **Er-Cl-Y** and **Elastosil®Film** (c) and the elastic moduli at different strains for **E2-X-Y** (d), **E3-X-Y** (e) and **Er-Cl-Y** and **Elastosil®Film** (f). The stress-strain curves were averaged from three independent samples. The strain at break is the minimum value obtained from the three tests.

All materials **En-X-Y** were investigated in electromechanical tests using circular electrodes. As reference the commercially available PDMS elastomer **Elastosil®Film** was used. The films were bilaterally

prestrained by 7.5% and fixed between two rigid plastic frames (Φ = 25 mm). Electrodes consisting of carbon black powder were smeared on both sides (Φ = 8 mm). Figure 6 gives the lateral actuation strain as function of applied electric field, while Table 5 summarizes the actuation sensitivity ($\varepsilon'/Y_{10\%}$) as well as the maximum actuation s_{max}, actuator breakdown E_b, lateral actuation at 10 V μm^{-1}, and thickness. It should be mentioned that due to out-of-plane deformation, *i.e.* buckling which typically set in at actuations above 10%, the lateral actuation cannot be accurately measured. Thus, the measured lateral actuation above 10% is underestimated (Figure 6, see videos ESI).

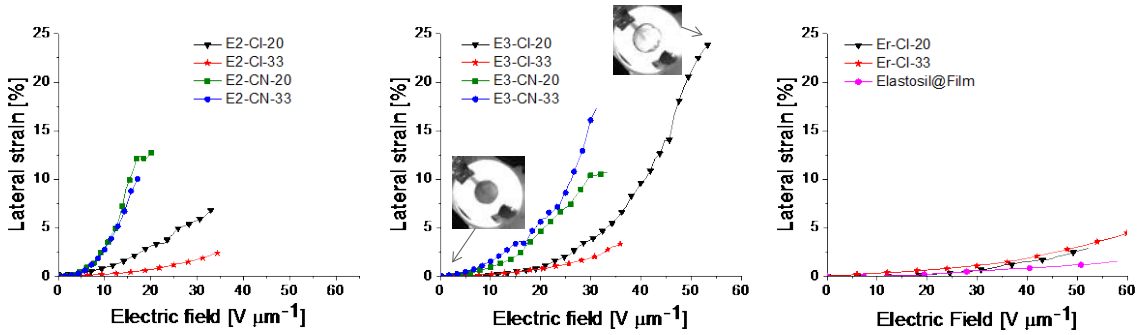

Fig. 6 Lateral actuation as a function of the applied electric field of materials **E2-X-Y** (left), of **E3-X-Y** (middle) with photos of the actuator constructed from **E3-Cl-20** in the relaxed state and actuated at an electric field of 53 V μm^{-1} whereby out of plane deformation dome shape was observed (middle), and **Er-Cl-Y** and **Elastosil®Film** (right). The elastomeric films were prestrained by 7.5%.

Because materials **E2-CN-Y** were softer and had a slightly higher permittivity as compared to **E3-CN-Y**, they actuated at lower electric field. The highest lateral actuation strain of 12% at the lowest electric field of 17 V μm^{-1} was achieved for material **E2-CN-20**. It should be noted that the elastic moduli of **E2-CN-Y** only slightly changed with strain, while for materials **E3-CN-Y** an increase of the elastic moduli at strains higher than 25% was observed. Because materials **E3-CN-**Y were stiffer as compared to **E2-CN-Y**, they actuated at higher electric fields (Figure 6). The rather low dielectric breakdown field of the actuators constructed from **En-CN-Y** is likely due to the increased conductivity of these materials. All materials **En-Cl-Y** showed rapid stiffening above a certain strain which may allow suppressing EMI. As we were limited by the maximum voltage of 5600 V of our voltage source, the dielectric breakdown of actuators constructed from **En-Cl-Y** was not reached. Materials **En-Cl-20** were softer as compared to **En-Cl-33** and actuated at lower electric field. For example, material **E2-Cl-20** gave a maximum lateral actuation strain of 6.5% at 33 V μm^{-1}, while material **E3-Cl-20** gave only 3.5% lateral actuation at an

electric field of 36 V μm^{-1}. Material **E3-Cl-20** allowed construction of actuators that were capable of suppressing EMI and for which ultra-large actuations were measured. An accurate measurement of the lateral actuation strain was not possible, as out of plane deformation occurred (Figure 6 middle). This material could be repeatedly actuated at 53 V μm^{-1} without degradation (see video in ESI). Considering the actuation shape a half sphere, the areal actuation strain was estimated using the measured lateral actuation strain of 24% at 53 V μm^{-1}. With this assumption, an area actuation strain of about 200% was calculated.

Table 5. Maximum actuation strain s_{max}, dielectric breakdown of actuator $E_{b,act}$, lateral actuation strain at 10 V μm^{-1}, the electromechanical sensitivity $\varepsilon'/Y_{10\%}$, and the film thickness d.

Sample	$\varepsilon'/Y_{10\%}$ [MPa^{-1}]	$s_{(max)}$ [%]	$E_{b,act}$ [a)] [V/µm]	s @ 10V/µm [%]	d [µm]
E3-Cl-20	15	24	53 [b)]	0.2	105
E3-CN-33	25	17.5	31	1.5	180
E2-CN-20	34	12	19	3	130
E3-CN-20	19	10	33	1	150
E2-CN-33	28	10	17	3	140
E2-Cl-20	18	6.5	33 [b)]	0.2	170
E3-Cl-33	10	3.5	36 [b)]	0.2	155
E2-Cl-33	9	2.5	35 [b)]	0.2	160
Er-Cl-33	6	5.5	64	0.3	50
Er-Cl-20	6	3	50	0	65
Elastosil ®Film	3	2.5	59 [b)]	0	95

[a]7.5% bilateral prestrain was applied. [b]No electric breakdown occurred.

The processability of **E3-Cl-20** in thin films was further optimized. To achieve more uniform films, a sacrificial layer of polyvinyl alcohol deposited on a glass plate was used, on which the new material was cross-linked. The formed material **E3-Cl-20*** had very similar dielectric properties to the previous one, but was slightly softer, *e.g.* **E3-Cl-20*** had a $Y_{10\%} = 260$ kPa, while **E3-Cl-20** had a $Y_{10\%} = 370$ kPa, respectively. In an attempt of getting accurate actuation measurements, **E3-Cl-20*** was tested at different biaxial prestains (0%, 22.5%, and 30%). Also here an accurate measurement of actuation was not possible. For actuators constructed from films that were biaxially prestrained by 22.5% and 30%, out of plane deformation occurred when the lateral actuation was above 10% (Figure 7). When no mechanical prestrain was used, out-of-plane actuation occurred from the very beginning. No dielectric breakdown was observed in all actuators constructed from **E3-Cl-20***, irrespective of the applied prestrain. High lateral actuation of 21% (more than 150% area actuation) at an electric field of 40 V μm^{-1} of actuators constructed from un-prestrained **E3-Cl-20*** were measured. This result indicates that **E3-Cl-**

20* is capable of achieving high actuation strain without prestrain while completely suppressing EMI. Photos and a movie of an actuator constructed from an un-prestrained **E3-Cl-20*** film (Figure 7 middle, right) clearly show the huge out of plane deformation at 42 V µm^{-1} (see supporting information).

Fig. 7 Lateral actuation strain **E3-Cl-20*** as function of the applied electric field (left) and photos of the actuator prepared from unprestrained films at 0 V µm^{-1} (middle) and at 42 V µm^{-1} (right). No dielectric breakdown occurred in actuators.

The leakage current during actuation is a very important material parameter as this current is converted into heat and thus may influence the reliability and life time of DEA.[23] While for single membrane actuator, efficient dissipation of heat may occur, this process is slowed down in stacked actuators and therefore the impact of leakage current is expected to be even more important. The leakage current of the new material was found to be low, comparable to the one measured for **Elastosil®Film**. An actuator constructed from **E3-Cl-20*** 22.5% prestrained showed a leakage current of 1 µA at an electric field of 27 V µm^{-1}. At this field a lateral actuation strain of 10% was measured. When increasing the electric field to 42 V µm^{-1} an increase in the leakage current to 4 µA was observed.

The electromechanical response speed was demonstrated by cyclic actuation tests at frequencies ranging from 0.5 Hz to 8 Hz performed using a 30% prestrained film. This prestrain was selected to minimize the measurement error due to buckling (Figure 8, left). For each frequency, 100 cycles were conducted. A slight decrease of the actuation with increasing actuation frequency was observed, *e.g.* at 0.5 Hz an actuation strain of 22% was measured, while at 8 Hz the actuation decreased to 20%. It should be noted that at higher frequencies (4 and 8 Hz), the actuator constructed from our new material did not completely recover the initial shape after discharging, about 5% remnant strain was observed, but the actuation strain was the same for consecutive cycles. Thus, a lateral actuation strain of 15% was measured. **Elastosil®Film** showed no limit of response speed. Due to the low dielectric permittivity,

Elastosil®Film showed a maximum actuation strain of only 8% at an electric field as high as 90 V µm^{-1} (Figure S61).

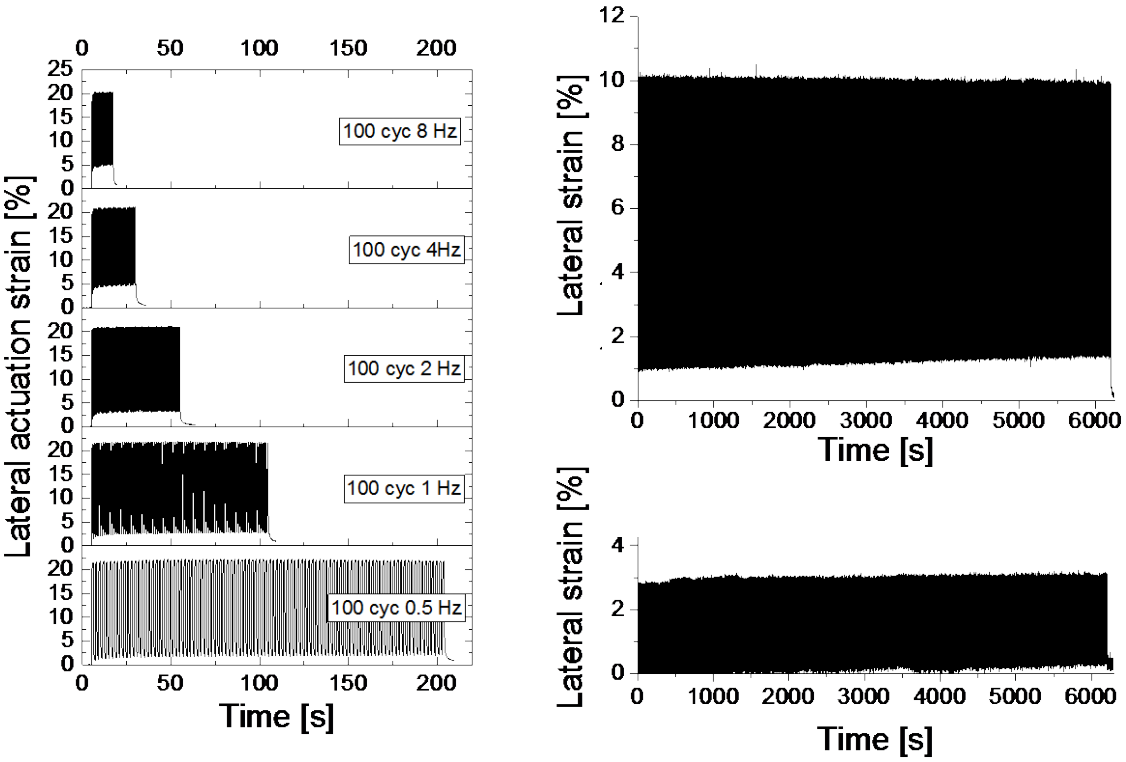

Fig. 8 100 actuation cycles at 0.5-8 Hz and an electric field of 42 V µm^{-1} of **E3-Cl-20*** prestrained by 30% (left), 50.000 actuation cycles at 8 Hz and an electric field of 27 V µm^{-1} of **E3-Cl-20*** (top right), and 50.000 actuation cycles at 8 Hz and 67 V µm^{-1} of **Elastosil®Film** prestrained by 22.5% (bottom right).

Cyclic actuation measurement of **E3-Cl-20*** over 50.000 cycles at 8 Hz showed a constant actuation of about 10% at 27 V µm^{-1} and a leakage current density of 0.5 µA cm^{-2} (Figure 8 right). Cyclic actuation of **Elastosil®Film** over 50.000 cycles at 8 Hz showed a lateral actuation strain of 3% at 67 V µm^{-1} and a leakage current density of 0.5 µA cm^{-2}. Due to the increased permittivity, good mechanical properties with low mechanical losses, excellent, fast, and reliable actuation at electric fields where leakage current is very low, this material can be considered as a promising replacement for regular PDMS. Further work is invested in improving the processability of thin films in order to prepare stacked actuators.

Conclusions

Grafting of alkyl thiols to polymethylvinylsiloxane has been shown to be an effective approach to polymers with increased permittivity. Appropriate cross-linking allowed formation of elastomers with

excellent insulating properties and high actuation strain. A synergetic effect between the thioether side groups of the polymer and the *in situ* generated silsesquioxane reflected by a rapid stiffening of the materials above a certain strain is desirable to suppress electromechanical instability and to achieve large actuation strains. A novel dielectric elastomer material was achieved starting from a silanol end-terminated polysiloxane modified with propyl-thioether side groups and 3-chloropropyl(triethoxy)silane. The material showed relative permittivity of $\varepsilon' = 5.4$ which was attributed to the presence of sulfur and chlorine in our material. The material shows a conductivity of $\sigma = 4\times10^{-11}\,\mathrm{S\,cm^{-1}}$ and good mechanical properties with a storage modulus of 300 kPa and a loss factor below 0.1, but a uniaxial strain at break of 100%. The stiffening of the material at rather low strains completely suppressed electromechanical instability and prevented the dielectric from premature breakdown. Area actuation strain of about 200% was calculated at an electric field of $53\,\mathrm{V\,\mu m^{-1}}$. This large actuation was possible due to the sharp stiffening of the elastomer above a certain strain. Additionally, the material could be actuated for more than 50.000 times at 8 Hz and gave a stable lateral actuation strain of 10% at an electric field of $27\,\mathrm{V\,\mu m^{-1}}$ with a leakage current density of $0.5\,\mu\mathrm{A\,cm^{-2}}$.

Because of the attractive dielectric characteristics and actuation behavior, this material recommends itself as a future replacement for regular PDMS elastomers. The increased permittivity allows for a reduction of driving voltage of actuators, an increased energy density in generators, and an increased sensitivity of sensors. Further work is devoted in implementing this class of materials in printable stacked devices.

Conflicts of interest

There are no conflicts to declare.

Acknowledgements

We gratefully acknowledge SNF (SNF142215, SNF206021_150638/1 and SNF172693) and Swiss Federal Laboratories for Materials Science and Technology (Empa, Dübendorf) for financial support. We also acknowledge B. Fischer (Empa) for DSC, TGA, and GPC measurements, T. Kuenniger (Empa) for her support with the DMA measurements, B. Geyer for his support with the movies, and L. Düring (CT System) and G. Kovacs (Empa) for their support with the actuator measurements.

Notes and references

1 R. Pelrine, R. Kornbluh, Q. Pei and J. Joseph, *Science*, 2000, **287**, 836.

2 Q. Pei, M. A. Rosenthal, R. Pelrine, S. Stanford and R. Kornbluh, *Proc. SPIE*, 2003, **5051**, 281.

3 C. Jordi, S. Michel, G. Kovacs and P. Ermanni, *Sens. Actuators A*, 2010, **161**, 182.

4 O. A. Araromi and S. C. Burgess, *Smart Mater. Struct.* 2012, **21**, 032001.

5 F. M. Weiss, H. Deyhle, G. Kovacs and B. Mueller, *Proc. SPIE*, 2012, **8340**, 83400A.

6 R. D. Kornbluh, R. E. Pelrine, H. Prahlad, S. Chiba, J. S. Eckerle, B. Chavez, S. E. Stanford and T. Low, *US 7557456*, 2007.

7 F. Carpi, Electromechanically active polymers, Springer, 2016.

8 A. Tröls, A. Kogler, R. Baumgartner, R. Kaltseis, C. Keplinger, R. Schwödiauer, I. Graz and S. Bauer, *Smart. Mater. Struct.* 2013, **22**, 104012.

9 J. S. Plante and S. Dubowsky, *Int. J. Solids Struct.* 2006, **43**, 7727.

10 X. Zhao and Z. Suo, *Appl. Phys. Lett.* 2007, **91**, 061921.

11 X. Zhao and Z. Suo, *Phys. Rev. Lett.* 2010, **104**, 1.

12 M. Moscardo, X. Zhao, Z. Suo and Y. Lapusta, J. Appl. Phys. 2008, **104**, 093503

13 T. Lu, J. Huang, C. Jordi, G. Kovacs, R. Huang, D. R. Clarke and Z. Suo, *Soft Matter*, 2012, **6**, 6167.

14 R. Pelrine, R. Kornbluh, J. Joseph, R. Heydt, Q. Pei and S. Chiba, *Mater. Sci. Eng. C*, 2000, **11**, 89.

15 J. Huang, T. Li, C. C. Foo, J. Zhu, D. R. Clarke and Z. Suo, *Appl. Phys. Lett.* 2012, **100**, 041911.

16 C. Keplinger, T. Li, R. Baumgartner, Z. Suo and S. Bauer, *Soft Matter*, 2012, **8**, 285.

17 T. Li, C. Keplinger, R. Baumgartner, S. Bauer, W. Yang and Z. Suo, *J. Mech. Phys. Solids*, 2013, **61**, 611.

18 S. M. Ha, M. Wissler, R. Pelrine, S. Stanford, G. Kovacs and Q. Pei, *Proc. SPIE*, 2007, **6524**, 652408.

19 C. Jordi, A. Schmidt, G. Kovacs, S. Michel and P Ermanni, *Smart Mater. Struct.* 2011, **20**, 075003.

20 X. Niu, H. Stoyanov, W. Hu, R. Leo, P. Brochu and Q. Pei, *J. Polym. Sci., Part B: Polym. Phys.* 2013, **51**, 197.

21 P. Brochu, H. Stoyanov, X. Niu and Q. Pei, *Smart Mater. Struct.* 2013, **22**, 0550227.

22 R. Shankar, T. K. Ghosh and R. J. Spontak, *Adv. Mater.* 2007, **19**, 2218.

23 R. Shankar, T. K. Ghosh and R. J. Spontak, *Macromol. Rapid Commun.* 2007, **28**, 1142.

24 M. Vatankhah-Varnoosfaderani, W. F. M. Daniel, A. P. Zhushma, Q. Li, B. J. Morgan, K. Matyjaszewski, D. P. Armstrong, R. J. Spontak, A. V. Dobrynin and S. S. Sheiko, *Adv. Mater.* 2017, **29**, 1604209.

25 D. M. Opris, *Adv. Mater.* 2018, **30**, 17036778.

26 P. Brochu and Q. Pei, *Macromol. Rapid Commun.* 2010, **31**, 10.

27 L.J. Romasanta, M.A. Lopez-Manchado and R. Verdejo, *Prog. Polym. Sci.* 2015, **51**, 188.

28 F. B. Madsen, A. E. Daugaard, S. Hvilsted and A. L. Skov, *Macromol. Rapid Commun.* 2016, **37**, 378.

29 D. Opris, S. Dünki and F. Nüesch, *J. Mater. Chem. C*, 2016, **4**, 10545.

30 L. Zhang, D. Wang, P. Hu, J.-W. Zha, F. You, S.-T. Li and Z.-M. Dang, *J. Mater. Chem. C*, 2015, **3**, 4883.

31 F. B. Madsen, L. Yu, A. E. Daugaard, S. Hvilsted and A. L. Skov, *RSC Adv.* 2015, **5**, 10254.

32 M. Stepp, F. Achenbach and A. Koellnberger*, PCT Int. Appl., WO 2015/121261 A1 20150820*, 2015.

33 S. J. Dünki, M. Dascalu, F. A. Nüesch and D. M. Opris, *Proc. SPIE*, 2016, **9798***,* 97982K.

34 S. J. Dünki, M. Tress, F. Kremer, S. Y. Ko, F. A. Nüesch, C.-D. Varganici, C. Racles and D. M. Opris, *RSC Adv.* 2015, **5**, 50054.

35 L. Maffli, S. Rosset, M. Ghilardi, F. Carpi and H. Shea, *Adv. Funct. Mater.* 2015, **25**, 1656.

36 J. E. Q. Quinsaat, M. Alexandru, F. A. Nüesch, H. Hofmann, A. Borgschulte and D. M. Opris, *J. Mater. Chem. A*, 2015, **3**, 14675**.**

37 M. Cazacu, M. Ignat, C. Racles, M. Cristea, V. Musteata, D. Ovezea and D. Lipcinski, *J. Compos. Mater.* 2014, **48**, 1533.

38 M. Alexandru, M. Cazacu, A. Nistor, V. E. Musteata, I. Stoica, C. Grigoras and B. C. Simionescu, *J. Sol-Gel Sci. Techol.* 2010, **56**, 310.

39 A. Bele, M. Cazacu, C. Racles, G. Stiubianu, D. Ovezea and M. Ignat, *Adv. Eng. Mater.* 2015, **17**, 1302.

40 A. Bele, M. Dascalu, C. Tugui, M. Iacob, C. Racles, L. Sacarescu and M. Cazacu, *Mater. Des.* 2016, **106**, 454.

41 S. J. Dünki, E. Cuervo-Reyes and D. M. Opris, *Polym. Chem.* 2017, **8**, 715.